Pergamon

J. Mech. Phys. Solids, Vol. 46, No. 11, pp. 2233–2259, 1998

Printed in Great Britain
0022–5096/98 $—see front matter

PII: S0022–5096(98)00003–9

INTERSONIC CRACK GROWTH IN BIMATERIAL INTERFACES: AN INVESTIGATION OF CRACK FACE CONTACT

Y. HUANG,*† W. WANG,¶ C. LIU‡ and A. J. ROSAKIS§

†Department of Mechanical and Industrial Engineering, University of Illinois at Urbana-Champaign, Urbana, IL 61801, U.S.A.; ‡MST-8, Material Research and Processing Science, Material Science and Technology Division, Mail Stop: G755, Los Alamos National Laboratory, Los Alamos, NM 87545, U.S.A.; §Graduate Aeronautical Laboratories, California Institute of Technology, Pasadena, CA 91125, U.S.A.; ¶ Department of Engineering Analysis, CASE Technical Center, 75.600 County Line Road, Burr Ridge, IL 60521, U.S.A.

(*Received* 18 *April* 1997; *in revised form* 6 *January* 1998)

ABSTRACT

Steady-state intersonic interfacial crack growth accounting for crack face contact is analyzed. The results clearly predict the essential features of experimental observations based on two different but complementary optical techniques and high speed photography. The solution features a large scale contact zone and two distinct traveling shock waves, one emanating from the crack tip and the other from the end of the contact zone. In addition, the solution predicts a non-zero energy dissipation rate due to crack face contact. © 1998 Elsevier Science Ltd. All rights reserved

Keywords: intersonic crack growth, bimaterial interface, crack face contact.

1. INTRODUCTION

There have been numerous studies on dynamic interfacial fracture in the sub-Rayleigh regime, i.e., the regime where the interfacial crack tip speed is lower than the Rayleigh wave speed of each constituent in the bimaterial system (e.g., Gol'dstein, 1967; Willis, 1971, 1973; Brock and Achenbach, 1973; Atkinson, 1977; Wu, 1991; Yang *et al.*, 1991; Deng, 1992; Liu *et al.*, 1993). Atkinson (1977) claimed that the terminal speed of an interfacial crack should be the lower of the two Rayleigh wave speeds of constituents in a bimaterial, while Willis (1973) argued that the terminal speed should be slightly larger than the lower Rayleigh wave speed. However, Tippur and Rosakis (1991), Liu *et al.* (1993), Lambros and Rosakis' (1995) recent experimental studies showed some surprising phenomena in dynamic interfacial fracture. For a PMMA/Steel bimaterial, the interfacial crack tip speed was observed to rapidly approach and exceed not only the Rayleigh wave speed, but also the shear wave speed of PMMA. Motivated by the earliest of these experimental observations, Yang *et al.* (1991) conducted a steady-state asymptotic analysis of subsonic interfacial crack growth in

* To whom correspondence should be addressed.

the bimaterial. One purpose of the analysis was to investigate the limiting behavior of the crack tip energy release rate as the crack tip speed approaches the lower Rayleigh wave speed of the bimaterial. They found that, unlike crack growth in homogeneous materials, this limit remains bounded. As a result, it was shown to be theoretically possible for an interfacial crack tip to exceed this limit, which, in fact, was consistent with experimental results.

These new experimental observations have motivated a series of analytical studies on the nature of asymptotic fields near an intersonically propagating interfacial crack tip. Yu and Yang (1994) obtained the anti-plane shear (mode III) near-tip field for the crack tip speed between the shear wave speeds of the two constituents, though there has never been any experimental evidence of mode III intersonic interfacial crack growth. Indeed for the two extreme cases of bimaterials, i.e., when the two constituents are identical and when one constituent becomes rigid (i.e., elastic/rigid bimaterial system), Huang *et al.* (1996) established that intersonic anti-plane shear (mode III) crack propagation is inadmissible.

Motivated by experimental observations for the PMMA/Steel bimaterial under in-plane deformation conditions, Liu *et al.* (1995), Yu and Yang (1995), Huang *et al.* (1996) investigated the near-tip fields around an intersonically propagating interfacial crack tip whose crack faces remain traction-free. They showed that stresses are singular not only at the crack tip, but also on an entire ray propagating with the crack tip. This ray, similar to a shock wave in aerodynamics, represents a line of strong discontinuity and has been observed in a series of experimental studies (Liu *et al.*, 1993; Lambros and Rosakis, 1995; Singh *et al.*, 1997).

These experiments, however, also showed that a relatively large contact zone exists behind the crack tip. The contact zone length was between 1.5–2 mm. This is not of the small scale oscillatory contact type described by Rice (1988) for quasi-static interfacial fracture. This finite contact zone, propagating with the crack tip, results from the shear dominated nature of intersonic interfacial fracture (Lambros and Rosakis, 1995; Liu *et al.*, 1995). Based on an energy consideration, Lambros and Rosakis (1995) and Liu *et al.* (1995) concluded, for the PMMA/Steel bimaterial, that crack face contact should occur when the interfacial crack tip speed is between c_s^{PMMA} and $\sqrt{2}c_s^{\mathrm{PMMA}}$, where c_s^{PMMA} is the shear wave speed of PMMA. This range of interfacial crack tip speed is consistent with the observed crack face contact in Liu *et al.*'s (1993) and Lambros and Rosakis' (1995) experiments using the optical method of CGS (coherent gradient sensing), and is later confirmed by photoelasticity experiments (Singh *et al.*, 1997). Crack face contact and the existence of shock wave type stress discontinuities traveling with the crack tip have also been observed in the numerical simulations of Xu and Needleman (1996).

Finite contact behind the propagating crack tip raises the possibility of two shock waves being generated at the moving crack tip and at the end of the contact zone. Indeed, the most recent experimental observations based on photoelasticity clearly show the existence of two such shock waves when cracks propagate with a velocity in the range between c_s and $\sqrt{2}c_s$, where c_s is the shear wave speed of the more compliant constituent. In addition, the experiments clearly show that the two shock waves are equally inclined to the interface and indeed propagate with the same speed for substantial time periods throughout the experiments (Singh *et al.*, 1997).

Motivated by the aforementioned experimental and numerical observations, this paper presents an investigation of the stress field around an intersonically propagating interfacial crack tip with finite crack face contact. This is a generalization of our previous work on the intersonic bimaterial problem without crack face contact. The current work emulates the clear experimental evidence of the crack face contact, the appearance of two distinct shock waves, and provides a means for analyzing the experimentally obtained fringe patterns.

In Section 2, the method of analytical continuation is used to establish a general approach for intersonic interfacial crack growth under in-plane deformation conditions. Section 3 presents the asymptotic structure of near-tip fields with interfacial crack face contact, while Section 4 gives an analytical solution for a finite crack face contact zone. Results of comparison with both CGS and photoelasticity experiments are presented in Section 5. Calculations of the energy dissipation rate associated with crack face contact are given in Section 6. It should be noted here that the crack tip energy release rate of all previous intersonic homogeneous as well as interfacial solutions, which do not account for crack face contact, is zero for the entire intersonic crack tip velocity regime ($c_s < v < c_l$, where c_l is the longitudinal wave speed). In the present solution, the crack tip energy release rate is also zero. However, energy dissipated by crack face contact over the finite contact zone trailing the crack tip, as a result, a non-vanishing, net, energy dissipation rate occurs. This is consistent with the predictions of non-zero energy dissipation rate in shear-dominated intersonic crack growth in homogeneous solids by Broberg (1989).

Since the elastic moduli of steel are almost two orders of magnitudes higher than those of PMMA, the deformation and stress fields are rather similar to those in an elastic solid bonded to a rigid substrate (Liu *et al.*, 1995; Huang *et al.*, 1996). Furthermore, Huang *et al.* (1996) showed that an elastic/rigid bimaterial system can capture all characteristic features of a general elastic/elastic bimaterial, but the solution of the former is significantly simpler than that of the latter. Accordingly, analyses in the following sections are limited to an elastic/rigid bimaterial system undergoing plane stress or plane strain deformation. The solution for a general elastic/elastic bimaterial can be found in Wang *et al.* (1997).

2. MODELING OF INTERSONIC INTERFACIAL CRACK GROWTH WITH CRACK FACE CONTACT

A general formulation for a crack propagating intersonically along an interface between an elastic solid bonded to a rigid substrate under in-plane (plane strain or plane stress) deformation is given in this section. It is the basis for the asymptotic analysis in Section 3 and the finite contact zone solution in Section 4.

As shown in Fig. 1, the interface between the elastic solid and the rigid substrate lies in the x_1 axis. The crack tip propagates in the positive x_1 direction at a speed v, such that,

$$c_s < v < c_l \tag{1}$$

for an intersonic crack growth, where $c_s = \sqrt{\mu/\rho}$ and $c_l = \sqrt{(\kappa+1)/(\kappa-1)}c_s$ are the

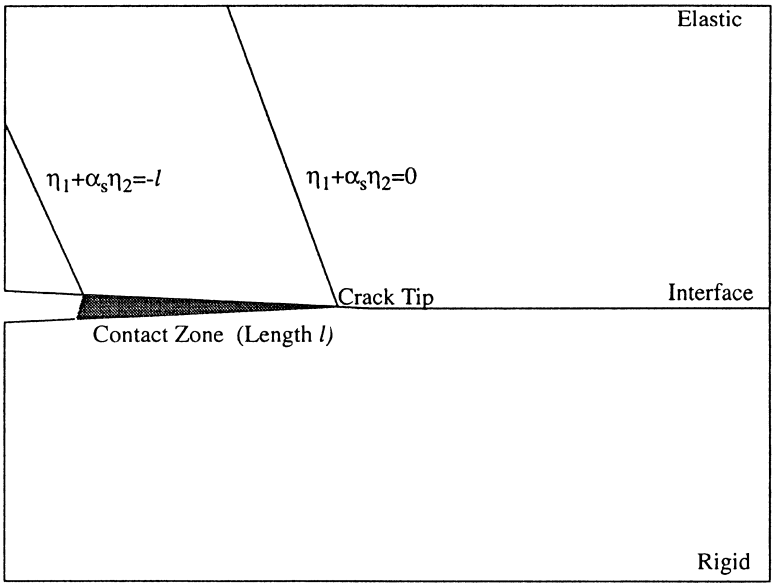

Fig. 1. An interface crack propagating intersonically between an elastic solid and a rigid substrate. There is a finite contact zone of length l at the elastic/rigid interface, trailing the crack tip. Two shock waves emanate from the crack tip and the end of the contact zone.

shear and longitudinal wave speeds, respectively, μ is the elastic shear modulus, ρ is the mass density, $\kappa = 3-4\nu$ for plane strain and $\kappa = (3-\nu)/(1+\nu)$ for plane stress, and ν is the Poisson's ratio. The in-plane displacements u_1 and u_2 in the elastic solid above the interface can be expressed by two displacement potentials ϕ and ψ as

$$u_1(x_1, x_2, t) = \frac{\partial}{\partial x_1}\phi(x_1, x_2, t) + \frac{\partial}{\partial x_2}\psi(x_1, x_2, t)$$

$$u_2(x_1, x_2, t) = \frac{\partial}{\partial x_2}\phi(x_1, x_2, t) - \frac{\partial}{\partial x_1}\psi(x_1, x_2, t). \tag{2}$$

The strains and stresses can be found in terms of displacement potentials from the strain–displacement and stress–strain relations. By introducing the moving coordinate $(\eta_1, \eta_2) = (x_1 - vt, x_2)$, and assuming the crack growth is steady-state, one finds that the equation of motion leads to a Laplace equation for ϕ and a wave equation for ψ (Freund, 1990), and they have the general solution (Liu *et al.*, 1995)

$$\left.\begin{aligned}\phi(\eta_1, \eta_2) &= \mathrm{Re}\,\{F(z_1)\}\\ \psi(\eta_1, \eta_2) &= g(\eta_1 + \hat{\alpha}_s\eta_2)\end{aligned}\right\} \quad \eta_2 > 0, \tag{3}$$

where $Re\{\cdot\}$ stands for the real part of a complex argument $z_1 = \eta_1 + i\alpha_l\eta_2$, $F(z_1)$ is an analytical function of z_1 in the upper half plane, $\eta_2 \geqslant 0$, $g(\eta_1 + \hat{\alpha}_s\eta_2)$ is a real function of its argument, and α_l and $\hat{\alpha}_s$ are given by

$$\alpha_1 = \left(1 - \frac{v^2}{c_1^2}\right)^{1/2} \quad \text{and} \quad \hat{\alpha}_s = \left(\frac{v^2}{c_s^2} - 1\right)^{1/2}. \tag{4}$$

Displacements and stresses in the elastic and solid above the interface can be expressed as

$$\left.\begin{aligned} u_1 &= \operatorname{Re}\{F'(z_1)\} + \hat{\alpha}_s g'(\eta_1 + \hat{\alpha}_s \eta_2) \\ u_2 &= -\alpha_1 \operatorname{Im}\{F'(z_1)\} - g'(\eta_1 + \hat{\alpha}_s \eta_2) \end{aligned}\right\} \quad \eta_2 > 0, \tag{5}$$

and

$$\left.\begin{aligned} \sigma_{11} &= \mu[(1 + 2\alpha_1^2 + \hat{\alpha}_s^2) \operatorname{Re}\{F''(z_1)\} + 2\hat{\alpha}_s g''(\eta_1 + \hat{\alpha}_s \eta_2)] \\ \sigma_{22} &= -\mu[(1 - \hat{\alpha}_s^2) \operatorname{Re}\{F''(z_1)\} + 2\hat{\alpha}_s g''(\eta_1 + \hat{\alpha}_s \eta_2)] \\ \sigma_{12} &= -\mu[2\alpha_1 \operatorname{Im}\{F''(z_1)\} + (1 - \hat{\alpha}_s^2) g''(\eta_1 + \hat{\alpha}_s \eta_2)] \end{aligned}\right\} \quad \eta_2 > 0, \tag{6}$$

where $\operatorname{Im}\{\cdot\}$ stands for the imaginary part of a complex argument.

At the interface ($\eta_2 = 0^+, \eta_1 > 0$), displacements should vanish because the elastic solid is bonded to a rigid substrate. This gives

$$\left.\begin{aligned} F'^{+}(\eta_1) + \bar{F}'^{-}(\eta_1) + 2\hat{\alpha}_s g'(\eta_1) &= 0 \\ \alpha_1[F'^{+}(\eta_1) - \bar{F}'^{-}(\eta_1)] + 2ig'(\eta_1) &= 0 \end{aligned}\right\} \quad \eta_1 > 0, \tag{7}$$

where $\bar{F}(z_1) = \overline{F(\bar{z}_1)}$ is an analytic function in the lower half plane of z_1, and superscript "$+$" and "$-$" stand for the limits for $\eta_2 \to 0^+$ and $\eta_2 \to 0^-$, respectively. By eliminating $g(\eta_1)$, one finds

$$(\alpha_1 \hat{\alpha}_s - i) F'^{+}(\eta_1) - (\alpha_1 \hat{\alpha}_s + i) \bar{F}'^{-}(\eta_1) = 0 \quad \eta_1 > 0. \tag{8}$$

Based on analytical continuation, a new analytic function $\theta(z)$ is introduced

$$\left.\begin{aligned} \theta(z) &= (\alpha_1 \hat{\alpha}_s - i) F'(z) \quad \operatorname{Im}(z) \geqslant 0 \\ \theta(z) &= (\alpha_1 \hat{\alpha}_s + i) \bar{F}'(z) \quad \operatorname{Im}(z) < 0 \end{aligned}\right\}. \tag{9}$$

The function $\theta(z)$ is analytic in the entire plane, except on the crack face ($\eta_2 = 0, \eta_1 < 0$). For $\eta_1 > 0$, the function $g(\eta_1)$ is related to $\theta(z)$ through Eqs. (7) and (9) by

$$g'(\eta_1) = -\frac{\alpha_1}{1 + \alpha_1^2 \hat{\alpha}_s^2} \theta(\eta_1) \quad \eta_1 > 0. \tag{10}$$

The above analysis holds for intersonic crack growth along an elastic/rigid interface under in-plane deformation conditions, regardless of the boundary conditions on the crack faces. For example, it holds for the traction-free crack face in Liu *et al.* (1995), as well as for infinite or finite contact zone solutions in Sections 3 and 4. The function $\theta(z)$ is the only function to be determined by the boundary conditions on the crack face. In the present study, a linear contact model is adopted such that the shear and normal stresses within the contact zone are related by

$$\sigma_{12} = \lambda \sigma_{22} \quad \eta_2 = 0^+, \tag{11}$$

where the linear contact coefficient λ is assumed to depend on bimaterial and bond properties. In general, this coefficient may be a function of sliding velocity as extensively discussed by Perrin *et al.* (1995). In addition, recent high rate experiments by Prakash and Clifton (1992, 1993) have revealed a strong velocity dependence of the frictional sliding process. However, in the present model, λ has been kept constant for simplicity.

It should be pointed out at this point that although the linear contact coefficient λ bears similarity with the friction coefficient, they are distinctly different because the cracked interface is rough and serrated by construction and causes microscale locking which gives large resistance against interfacial sliding. This interface locking can be better understood from the specimen preparation procedure. Similar to that proposed by Tippur and Rosakis (1991), and PMMA and metal were bonded together via an adhesive, which was a commercially available product consisting of two components: a Methylmethacrylate monomer (MMA) and a catalyst that can polymerize the monomer (Lambros and Rosakis, 1995). Each side to be bonded was roughened by sandblasting with 10–20 micron sized glass beads. The resulting bonding layer was roughly 100 microns in thickness and the cured adhesive material had the stiffness similar to that of PMMA. The same procedure was also adopted by Singh and Shukla (1996) in their bimaterial system composed of the Homalite-100 and aluminum. The bonding surfaces in both bimaterial systems were sandblasted, such that the roughness of bimaterial interfaces would be on the order of 10–20 microns. This artificial roughness produced a mechanical bond between the metal and polymer material constituents. A schematic diagram of the roughened interface is shown in Fig. 2, where the interface has a sinusoidal profile with the distance from peak to valley on the order of 10 microns and with the wavelength around 30 microns. As the interface is subjected to the shear-dominated loads as in intersonic crack propagation, the interface prevents the sliding of the material above the interface with respect to the material below the interface. This "interlocking" mechanism can lead to a large linear contact coefficient λ (e.g., $\lambda > 1$).

Because of the existence of a rigid constituent in the bimaterial, the normal displacement u_2 within the contact zone should vanish

$$u_2 = 0 \quad \eta_2 = 0^+. \tag{12}$$

The shear traction at the contact face should be resisting the relative sliding on the crack face. This gives

$$-\sigma_{12} v_1 < 0 \quad \eta_2 = 0^+, \tag{13}$$

where $-\sigma_{12}$ is the shear traction, and $v_1 = \mathrm{d}u_1/\mathrm{d}t$ is the particle velocity along the crack face.

3. THE STRUCTURE OF NEAR-TIP ASYMPTOTIC FIELD

In this section, we consider the solution of an intersonic interfacial crack problem involving semi-infinite contact. Alternatively, this can be thought as the asymptotic

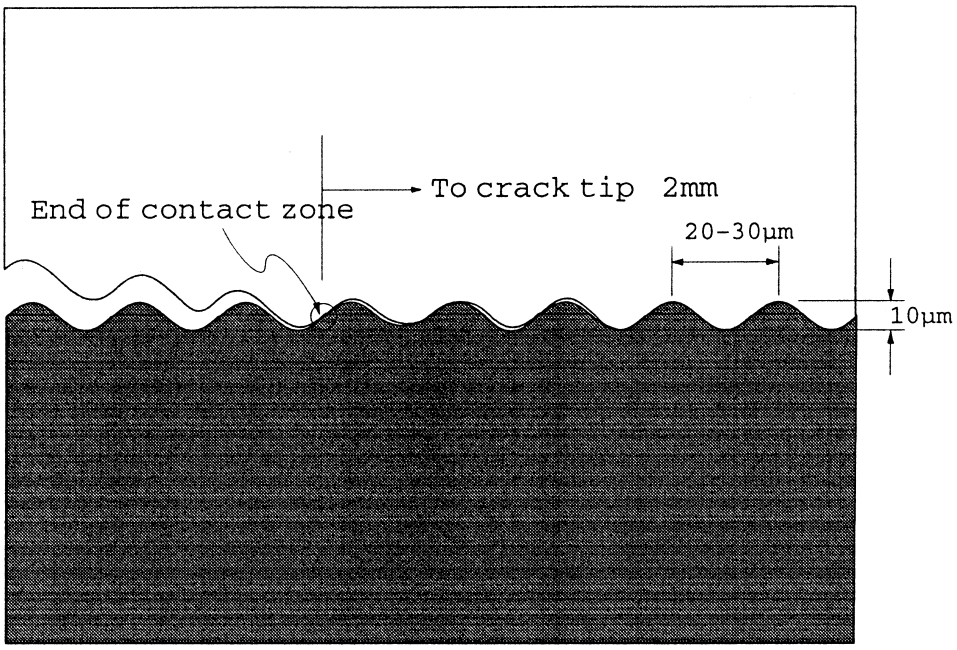

Fig. 2. A schematic diagram of the roughened interface; the interface has a sinusoidal profile with the distance from peak to valley on the order of 10 microns and with the wave length around 30 microns. As the interface is subjected to the shear-dominated loads as in intersonic crack propagation, the interface prevents the sliding of the material above the interface with respect to the material below the interface. This "interlocking" mechanism leads to a large linear contact coefficient λ (e.g., $\lambda > 1$).

problem corresponding to a case of a finite contact zone as the distance to crack tip vanishes. In the asymptotic analysis, the crack face contact conditions in (11) and (12) are used for the entire crack face ($\eta_1 < 0$). Accordingly, the substitution of displacements and stresses in Eqs. (5) and (6) into Eqs. (11) and (12) gives

$$\left.\begin{aligned} &2\alpha_1[F''^{+}(\eta_1)-\bar{F}''^{-}(\eta_1)]+2i(1-\hat{\alpha}_s^2)g''(\eta_1) \\ &=\lambda\{i(1-\hat{\alpha}_s^2)[F''^{+}(\eta_1)+\bar{F}''^{-}(\eta_1)]+4\hat{\alpha}_s i g''(\eta_1)\}\end{aligned}\right\} \quad \eta_1 < 0, \tag{14}$$

$$\alpha_1[F'^{+}(\eta_1)-\bar{F}'^{-}(\eta_1)]+2ig'(\eta_1)=0 \quad \eta_1 < 0. \tag{15}$$

By eliminating $g(\eta_1)$, one finds the relation between $F''^{+}(\eta_1)$ and $\bar{F}''^{-}(\eta_1)$ for $\eta_1 < 0$. In terms of the analytic function $\theta(z)$ in Eq. (9), it can be expressed as

$$\theta'^{+}(\eta_1)-\frac{(\alpha_1\hat{\alpha}_s-i)\{\alpha_1(1+\hat{\alpha}_s^2)+\lambda[2\alpha_1\hat{\alpha}_s+i(1-\hat{\alpha}_s^2)]\}}{(\alpha_1\hat{\alpha}_s+i)\{\alpha_1(1+\hat{\alpha}_s^2)+\lambda[2\alpha_1\hat{\alpha}_s-i(1-\hat{\alpha}_s^2)]\}}\theta'^{-}(\eta_1)=0 \quad \eta_1 < 0. \tag{16}$$

This constitutes a Riemann–Hilbert problem. The boundness for displacements near the crack tip requires $\theta'(z) = O(|z|^{\alpha})$ as $|z| \to 0$ for $\alpha > -1$. The general solution for $\theta'(z)$ is

$$\theta'(z) = \frac{A(z)}{z^q}, \tag{17}$$

where $A(z)$ is an entire function (analytic in the entire plane including the crack face), and the power of stress singularity q near the crack tip is given by

$$q = \frac{1}{\pi}\tan^{-1}\left\{\frac{\alpha_l(1+\hat{\alpha}_s^2)(1+\lambda\hat{\alpha}_s)}{\alpha_l^2\hat{\alpha}_s(1+\hat{\alpha}_s^2)+\lambda(1-\hat{\alpha}_s^2+2\alpha_l^2\hat{\alpha}_s^2)}\right\}. \tag{18}$$

This exponent depends on the crack tip velocity v, Poisson's ratio ν, and the linear contact coefficient λ. The power q is real, so that the near-tip stress field is not oscillatory for a crack tip propagating intersonically along an elastic/rigid interface with crack face contact. The power q becomes insensitive to λ for $|\lambda| > 10$, and is given by

$$q = \frac{1}{\pi}\tan^{-1}\left[\frac{\alpha_l\hat{\alpha}_s(1+\hat{\alpha}_s^2)}{1-\hat{\alpha}_s^2+2\alpha_l^2\hat{\alpha}_s^2}\right].$$

The function $F(z)$ can be obtained by substituting Eq. (17) into Eq. (9), which yields

$$F''(z) = \frac{1}{\alpha_l\hat{\alpha}_s - i}\frac{A(z)}{z^q} \quad \mathrm{Im}(z) \geqslant 0$$

$$\bar{F}''(z) = \frac{1}{\alpha_l\hat{\alpha}_s + i}\frac{A(z)}{z^q} \quad \mathrm{Im}(z) < 0. \tag{19}$$

Therefore,

$$\bar{A}(z) = A(z), \tag{20}$$

or in other words, if the entire analytic function $A(z)$ is expanded into Taylor series $A(z) = \Sigma_{n=0}^{\infty} A_n z^n$, all coefficients A_n $(n = 0, 1, 2, \ldots)$ are real. The dominant stress field in the asymptotic analysis corresponds to the leading term, A_0, in the Taylor expansion of $A(z)$. Similar to the Stress Intensity Factor in fracture mechanics, the real parameter A_0 represents the amplitude of the near-tip asymptotic field and depends on geometry of the bimaterial, time-varying external loading, and crack tip velocity. It is noted that the asymptotic stress field near an intersonic interface crack tip is governed by a single real parameter, while the corresponding field near a stationary or sub-Rayleigh interfacial crack tip is governed by a complex stress intensity factor.

The real function $g(\eta_1)$ can be obtained from (15) for $\eta_1 < 0$. In conjunction with Eq. (10), one finds

$$g''(\eta_1) = \begin{cases} -\dfrac{\alpha_l}{1+\alpha_l^2\hat{\alpha}_s^2}\dfrac{A_0}{\eta_1^q} & \eta_1 > 0 \\ -\alpha_l\dfrac{A_0}{(-\eta_1)^q}\dfrac{\cos q\pi - \alpha_l\hat{\alpha}_s\sin q\pi}{1+\alpha_l^2\hat{\alpha}_s^2} & \eta_1 < 0 \end{cases}. \tag{21}$$

The asymptotic displacement and stress fields near the crack tip are given in the Appendix. It is observed that stresses are singular not only at the crack tip, but also on the entire ray $\eta_1+\hat{\alpha}_s\eta_2=0$. Liu *et al.* (1995) have made similar observations in intersonic interfacial fracture without crack face contact. This ray of singularity propagating with the crack tip has been observed in experiments (Singh *et al.*, 1997), as discussed in detail in Section 5.

The field of particle velocity can be obtained from the displacement field by $v_i=-v\,\partial u_i/\partial\eta_1$ $(i=1,2)$, based on the assumption of steady-state crack growth. In particular, the particle velocity on the contact face is

$$v_1(\eta_1<0,\eta_2=0)=-vA_0\sin q\pi|\eta_1|^{-q}. \tag{22}$$

The requirement in Eq. (13) that the shear traction at the contact face is resisting crack face sliding becomes

$$\frac{\dfrac{\mu vA_0^2}{|\eta_1|^{2q}}\alpha_l^2(1+\hat{\alpha}_s^2)^2\lambda(1-\hat{\alpha}_s^2)(1+\lambda\hat{\alpha}_s)}{[\alpha_l^2\hat{\alpha}_s(1+\hat{\alpha}_s^2)+\lambda(1-\hat{\alpha}_s^2+2\alpha_l^2\hat{\alpha}_s^2)]^2+[\alpha_l(1+\hat{\alpha}_s^2)(1+\lambda\hat{\alpha}_s)]^2}>0, \tag{13'}$$

which gives the range of admissible linear contact coefficient λ as

$$\begin{aligned}
&\text{Region I} && c_s<v<\sqrt{2}c_s && \lambda>0\\
&\textit{Region II} && c_s<v<\sqrt{2}c_s && \lambda<-\left(\frac{v^2}{c_s^2}-1\right)^{-1/2}\\
&\textit{Region III} && \sqrt{2}c_s<v<c_l && -\left(\frac{v^2}{c_s^2}-1\right)^{-1/2}<\lambda<0.
\end{aligned} \tag{23}$$

This domain of admissible λ is shown in Fig. 3 vs the normalized crack tip velocity, v/c_s, i.e., the shaded regions marked by I, II and III in Fig. 3. Lambros and Rosakis (1995) and Liu *et al.* (1995) argued that crack face contact is expected when the crack tip velocity is between c_s and $\sqrt{2}c_s$. Equation (23) shows that any positive linear contact coefficient λ is admissible, as well as relatively large negative λ in the range, $|\lambda|>\alpha_s^{-1}(>1)$.

It should be pointed out that although the linear contact coefficient λ bears the similarity with the friction coefficient, the negative linear contact coefficient λ cannot be excluded for intersonic crack propagation. Once the deformation is in the intersonic regime, there are many phenomena that contradict to our physical intuition gained in the static or subsonic regimes. For example, Georgiadis and Barber (1993a, b) investigated the steady-state solution for a point load moving intersonically over an elastic half-plane. They established that, when the point load travels in the intersonic regime but below $\sqrt{2}c_s$, the normal displacement under the load becomes opposite to the load direction (the load is pushed up), which clearly contradicts to the intuitive picture for subsonic motion of the load. Even though it can be shown that the linear contact coefficient λ must be non-negative for subsonic crack propagation, it cannot be concluded at this point that λ is non-negative for intersonic crack propagation.

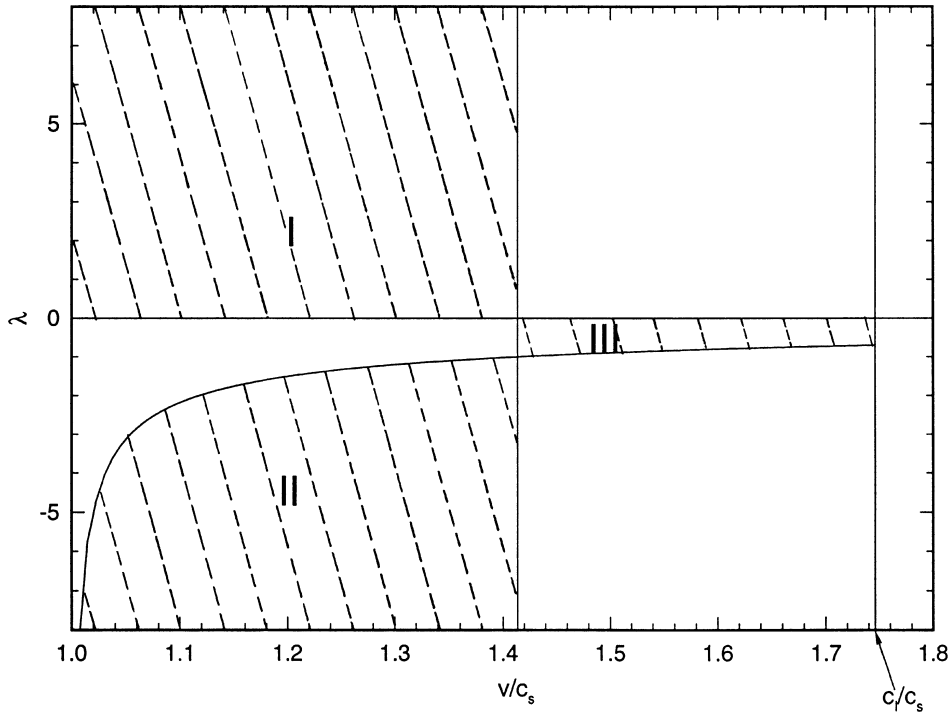

Fig. 3. The range of admissible linear contact coefficient λ vs the normalized crack tip velocity, v/c_s, for a plane-stress PMMA/rigid bimaterial system (Poisson's ratio $\nu_{PMMA} = 0.35$). Regions I, II and III correspond to $\lambda > 0$, $\lambda < -1$ and $-1 < \lambda < 0$, respectively.

The physical restriction on λ should be that it gives the shear traction at the contact face resisting the relative sliding on the crack face, as in Eq. (13).

The power of stress singularity q is shown in Fig. 4(a) vs the normalized crack tip velocity, v/c_s, in the range $c_s < v < \sqrt{2}c_s$ for crack face contact (Liu *et al.*, 1995), where the Poisson's ratio of PMMA, $\nu = 0.35$, and several positive linear contact coefficients λ are displayed. The power of stress singularity is less than 1/2 for the entire range of crack tip velocity. As a result, the energy flux into the crack tip (Freund, 1972, 1990) is zero. This phenomenon has also been observed in intersonic, shear-dominated fracture in both homogeneous and interface fracture (Freund, 1979; Broberg, 1989; Liu *et al.*, 1995; Yu and Yang, 1995; Huang *et al.*, 1996). However, the entire energy input from remote field is dissipated through the contact zone, as discussed in the next section. It is also observed that the stress singularity near the crack tip becomes weaker as the resistance against relative sliding increases (i.e., with increasing λ). All curves coincide at the same point in Fig. 4(a) when the crack tip velocity reaches $\sqrt{2}c_s$. The corresponding power of the crack tip singularity, $q = \tan^{-1}[(3-\kappa)/(1+\kappa)]^{1/2}/\pi$, is not only independent of λ, but also identical to Liu *et al.*'s (1995) solution which did not account for crack face contact. Indeed it can be easily verified that, at this critical velocity $\sqrt{2}c_s$, the solution of Liu *et al.* (1995) which predicted interpenetration at lower velocities, now predicts $u_2 = 0$. The present

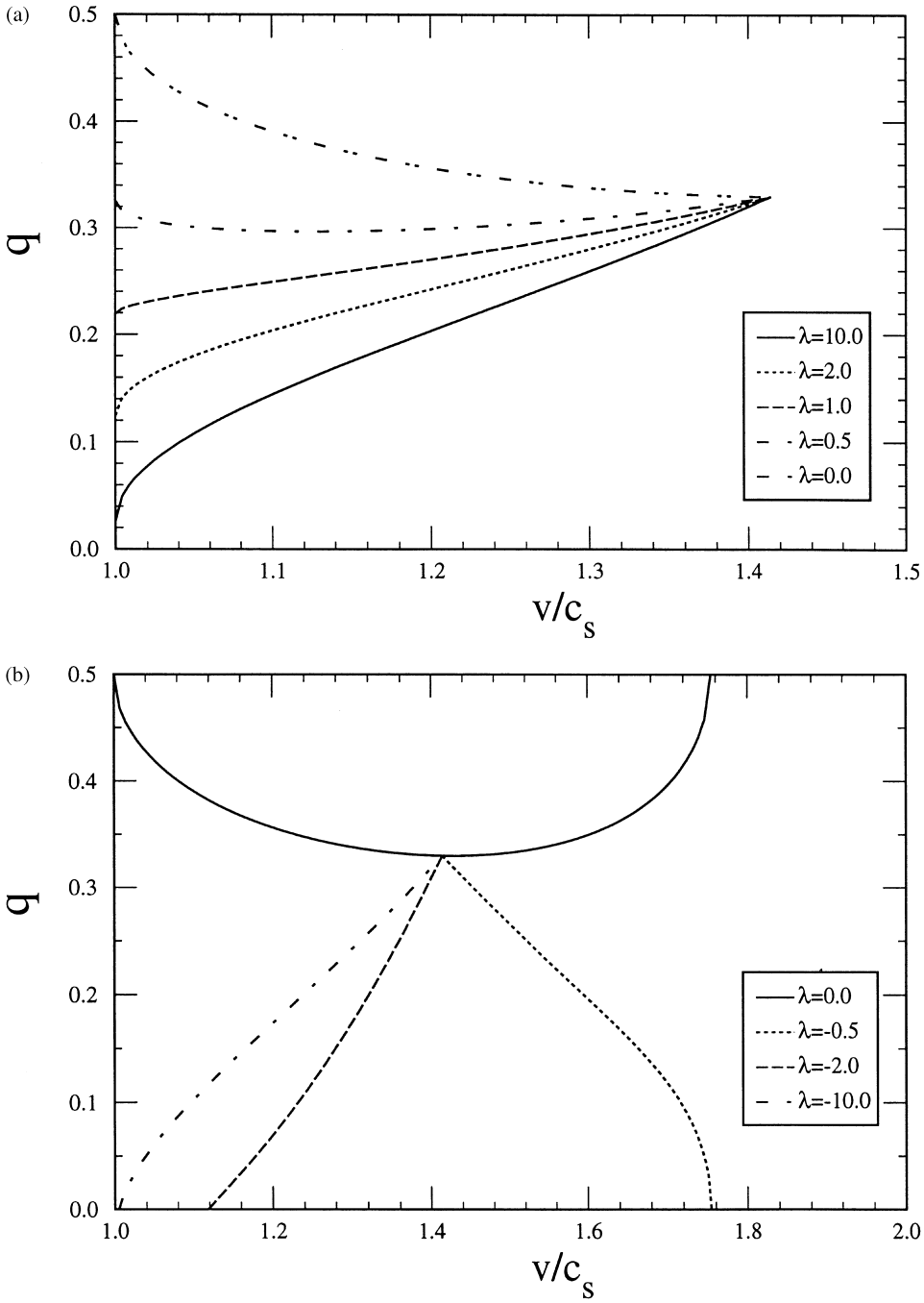

Fig. 4. The power of stress singularity q at the crack tip vs the normalized crack tip velocity, v/c_s, for a plane-stress PMMA/rigid bimaterial system (Poisson's ratio $\nu_{PMMA} = 0.35$): (a) positive linear contact coefficients λ; (b) admissible negative linear contact coefficients λ.

solution, which, in general, gives non-vanishing tractions in the contact zone at a lower crack tip velocity, now features zero tractions at this particular speed. Therefore, the transition from the present contact solution to Liu *et al.*'s field could occur smoothly at $v = \sqrt{2}c_s$; the crack tip propagates with crack face contact when $c_s < v < \sqrt{2}c_s$; the contact disappears and crack face opens once v reaches $\sqrt{2}c_s$. It should however be observed that the above scenario does not prove that crack face contact is impossible above $v = \sqrt{2}c_s$. Indeed the asymptotic solution features the undetermined amplitude A_0 whose sign will determine whether contact will occur for $v > \sqrt{2}c_s$.

This critical velocity $v = \sqrt{2}c_s$ is consistent with Georgiadis and Barber's (1993a, b) steady-state solution for a point load moving intersonically over an elastic half-plane. At $v = \sqrt{2}c_s$, the displacement on the boundary vanishes, even though a normal point load is applied at the boundary of the half-plane. Another interesting feature of this solution is that when the point load travels below $\sqrt{2}c_s$ but above the Rayleigh wave speed C_R the normal displacement under the load becomes opposite to the load direction (the load is pushed up), contradicting the expected intuitive picture which is true in the sub-Rayleigh motion of the load. This is indeed consistent with our general expectation of crack face contact in the $c_s < v < \sqrt{2}c_s$ velocity regime.

The power of stress singularity q is shown in Fig. 4(b) vs the normalized crack tip velocity for several admissible negative linear contact coefficients λ. Within the range $c_s < v < \sqrt{2}c_s$, the power of stress singularity q increases with resistance against relative sliding λ, which is contradictory to our physical intuition.

4. FINITE CONTACT ZONE AT THE INTERFACE

The asymptotic analysis in the previous section only holds near the crack tip. In order to compare with experimental observations in Liu *et al.* (1993), Lambros and Rosakis (1995), and Singh *et al.* (1997), the stress field is investigated in this section for a finite contact zone trailing an interface crack tip propagating intersonically. As shown in Fig. 1, the contact zone has a length l at the elastic/rigid interface. The contact conditions in Eqs. (11) and (12) hold within the contact zone, while a traction-free condition should be used for the crack face outside the contact zone, i.e.,

$$\sigma_{12} = \lambda\sigma_{22} \quad \text{and} \quad u_2 = 0 \quad -l < \eta_1 < 0, \tag{24}$$

and

$$\sigma_{12} = 0 \quad \text{and} \quad \sigma_{22} = 0 \quad \eta_1 < -l. \tag{25}$$

The contact conditions in Eq. (24) become identical to those in Eqs. (14) and (15) in terms of functions $F(\cdot)$ and $g(\cdot)$, except that they hold only for $-l < \eta_1 < 0$. Consequently, Eq. (16) also holds for $-l < \eta_1 < 0$.

The substitution of stresses in Eq. (6) into the traction-free conditions in Eq. (25) gives

$$\left.\begin{aligned}(1-\hat{\alpha}_s^2)\{F''^{+}(\eta_1)+\bar{F}''^{-}(\eta_1)\}+4\hat{\alpha}_s g''(\eta_1)=0\\ \alpha_1\{F''^{+}(\eta_1)-\bar{F}''^{-}(\eta_1)\}+i(1-\hat{\alpha}_s^2)g''(\eta_1)=0\end{aligned}\right\}\quad \eta_1<-l. \tag{26}$$

The elimination of function $g(\eta_1)$ yields a relation between F^+ and $\bar{F}^-$ outside the contact zone. In terms of the function $\theta(z)$ in Eq. (9), it can be expressed as

$$\theta'^{+}(\eta_1)-\frac{(\alpha_1\hat{\alpha}_s-i)[4\alpha_1\hat{\alpha}_s+i(1-\hat{\alpha}_s^2)^2]}{(\alpha_1\hat{\alpha}_s+i)[4\alpha_1\hat{\alpha}_s-i(1-\hat{\alpha}_s^2)^2]}\theta'^{-}(\eta_1)=0\quad \eta_1<-l. \tag{27}$$

Equations (16) (for $-l<\eta_1<0$) and (27) constitute a Riemann–Hilbert problem. However, the discontinuity conditions on the crack face are given separately inside the contact zone as in Eq. (16) and outside the zone as in Eq. (27). It is observed that the stress field has two singularities, one at the crack tip governed by Eq. (16) and the other at the end of contact zone ($\eta_1=-l, \eta_2=0$) determined by Eq. (27). The power of stress singularity at the crack tip should be the same as that in the asymptotic analysis in the previous section. The general solution for $\theta'(z)$ can be expressed as

$$\theta'(z)=\frac{B(z)}{z^q(z+l)^p}, \tag{28}$$

where $B(z)$ is an entire function, the power q represents the singularity at the crack tip, and the power p characterizes stress singularity at the end of the contact zone. Similar to Eq. (20), the entire function $B(z)$ satisfies $\bar{B}(z)=B(z)$. The substitution of above expression into the discontinuity condition (16) within the contact zone ($-l<\eta_1<0$) yields the identical solution for power q as in Eq. (18) because $(z+l)^{-p}$ is continuous across the contact zone. Its substitution into the traction-free condition in Eq. (27) gives the solution for $q+p$ because both z^{-q} and $(z+l)^{-p}$ are discontinuous outside the contact zone,

$$q+p=\frac{1}{\pi}\tan^{-1}\frac{\alpha_1\hat{\alpha}_s[4-(1-\hat{\alpha}_s^2)^2]}{4\alpha_1^2\hat{\alpha}_s^2+(1-\hat{\alpha}_s^2)^2}. \tag{29}$$

It is interesting to note that the above expression is independent of the linear contact coefficient λ, and is identical to the power of stress singularity in Liu *et al.* (1995) for an intersonically propagating interfacial crack without crack face contact. This is because Eq. (27) also holds on the crack face in Liu *et al.* (1995). When $|z|\gg l$, an observer is too far away to discern the contact zone, so that Eq. (28) degenerates to Liu *et al.*'s (1995) field without crack face contact. In other words, the power of stress singularity for a crack without crack face contact can be decomposed to two parts, the power at the crack tip and that at the end of the contact zone.

The power of stress singularity at the end of contact zone can be obtained by subtracting Eq. (18) from Eq. (29). This gives

$$p=\frac{1}{\pi}\tan^{-1}\left\{\frac{\alpha_1(1-\hat{\alpha}_s^4)[2\lambda\hat{\alpha}_s-(1-\hat{\alpha}_s^2)]}{4\alpha_1^2\hat{\alpha}_s(1+\hat{\alpha}_s^2)+\lambda[8\alpha_1^2\hat{\alpha}_s^2+(1-\hat{\alpha}_s^2)^3]}\right\}. \tag{30}$$

It depends on the crack tip velocity v, Poisson's ratio ν, and the linear contact

coefficient λ. The power p is also real, so that the stress near the end of contact zone may be singular (if p is positive) but not oscillatory.

The real function $g(\eta_1)$ can be obtained in terms of function $\theta(\eta_1)$ from Eqs. (15) and (26) for $-l < \eta_1 < 0$ and $\eta_1 < -l$, respectively. In conjunction with Eq. (10) and continuity of displacements at the end of the contact zone, one finds

$$g'(\eta_1) = \begin{cases} -\dfrac{\alpha_1}{1+\alpha_1^2\hat{\alpha}_s^2}\theta(\eta_1) & \eta_1 > 0 \\ \dfrac{i\alpha_1}{2}\left[\dfrac{\theta^+(\eta_1)}{\alpha_1\hat{\alpha}_s - i} - \dfrac{\theta^-(\eta_1)}{\alpha_1\hat{\alpha}_s + i}\right] & -l < \eta_1 < 0 \\ -\dfrac{1-\hat{\alpha}_s^2}{4\hat{\alpha}_s}\left[\dfrac{\theta^+(\eta_1)}{\alpha_1\hat{\alpha}_s - i} + \dfrac{\theta^-(\eta_1)}{\alpha_1\hat{\alpha}_s + i}\right] & \\ +\left(\dfrac{1-\hat{\alpha}_s^2}{4\hat{\alpha}_s} + \dfrac{i\alpha_1}{2}\right)\dfrac{\theta^+(-l)}{\alpha_1\hat{\alpha}_s - i} + \left(\dfrac{1-\hat{\alpha}_s^2}{4\hat{\alpha}_s} - \dfrac{i\alpha_1}{2}\right)\dfrac{\theta^-(-l)}{\alpha_1\hat{\alpha}_s + i} & \eta_1 < -l \end{cases} \tag{31}$$

where $\theta(z)$ is discontinuous across the crack face ($\eta_1 < 0$) and is given explicitly later in Eq. (36).

The function $B(z)$ in Eq. (28) can be expanded in Taylor series

$$B(z) = \sum_{n=0}^{\infty} B_n z^n, \tag{32}$$

where the coefficients B_n ($n = 0, 1, 2, \ldots$) are real. Its leading term B_0 corresponds to a stress field

$$\sigma_{ij} = \mu B_0 s_{ij}(\eta_1, \eta_2, q, p), \tag{33}$$

where s_{ij} are functions of positions (η_1, η_2) as well as powers of stress singularity q and p, and are given in the Appendix. It is observed that stresses are singular on two parallel rays, $\eta_1 + \hat{\alpha}_s\eta_2 = 0$ and $\eta_1 + \hat{\alpha}_s\eta_2 = -l$, starting at the crack tip and at the end of contact zone, respectively. This has been observed in Singh *et al.*'s (1997) photoelasticity experiments, as discussed in detail in the next section.

Although the high order terms in $B(z)$, e.g., $B_1 z$, $B_2 z^2$, $B_3 z^3, \ldots$, are relatively not important to stress field near the crack tip, they are crucial to the stress field near the end of contact zone. This is because these terms and the leading term B_0 are on the same order near $z = -l$. It is observed that the stress field associated with the real coefficient B_n can be simply obtained by changing q to $q-n$ in s_{ij}, and is given by $s_{ij}(\eta_1, \eta_2, q-n, p)$. Consequently, for general $B(z)$, the stress field becomes an infinite series given by

$$\sigma_{ij} = \mu \sum_{n=0}^{\infty} B_n s_{ij}(\eta_1, \eta_2, q-n, p), \tag{34}$$

where s_{ij} are given in the Appendix.

The displacement can also be obtained analytically and is shown below

$$u_1 = Re\left\{\frac{\theta(\eta_1 + i\alpha_l\eta_2)}{\alpha_l\hat{\alpha}_s - i}\right\} + \hat{\alpha}_s g'(\eta_1 + \hat{\alpha}_s\eta_2), \tag{35a}$$

$$u_2 = -\alpha_l Im\left\{\frac{\theta(\eta_1 + i\alpha_l\eta_2)}{\alpha_l\hat{\alpha}_s - i}\right\} - g'(\eta_1 + \hat{\alpha}_s\eta_2), \tag{35b}$$

where

$$\theta(z) = \sum_{n=0}^{\infty} B_n \int_0^z \xi^{n-q}(\xi + 1)^{-p}\,\mathrm{d}\xi, \tag{36}$$

and g' is given in Eq. (31). The velocity field can be found accordingly from the steady-state condition. Although the stress, displacement, and velocity fields are different from those in the asymptotic analysis in the previous section, it can be verified that the requirement in Eq. (13) for the shear traction at the contact face resisting crack face sliding leads to the identical range of admissible linear contact coefficient λ given in Eq. (23). This indicates that the range of admissible linear contact coefficient λ in the contact zone is intrinsic to the bimaterial system and crack tip speed.

The dependence of the power of stress singularity p at the end of contact zone on the normalized crack tip velocity, v/c_s, is shown in Fig. 5(a) for Poisson's ratio $\nu = 0.35$ and several positive linear contact coefficients λ. The power p is very small, typically less than 0.1, indicating a weaker stress singularity than that at the crack tip. For relatively large linear contact coefficient λ, there is a maximum value of p. It is noted that the exponent p can be negative for small λ, resulting in the lack of stress singularity and vanishing of the second shock wave emanating from the end of the contact zone.

In the event an admissible (Eq. (13)) negative λ occurs, the variation of exponent p is shown in Fig. 5(b) vs the crack tip speed.

5. COMPARISON WITH EXPERIMENTAL OBSERVATIONS

In this section, we present some qualitative comparisons of synthetically generated optical fringe patters to their experimental counterparts.

The optical method of Coherent Gradient Sensing (CGS) and the method of photoelasticity have been used in conjunction with high-speed photography (up to 2,000,000 frames per second) to record near-tip stress fields of intersonically moving crack tips in polymer/metal bimaterial systems (Lambros and Rosakis, 1995; Singh *et al.*, 1997). CGS fringes are contours of gradients of the first stress invariant (in-plane stress), i.e. they correspond to contours of equal $(\sigma_{11}+\sigma_{22})_{,1}$ or $(\sigma_{11}+\sigma_{22})_{,2}$ depending on the experimental setup. Photoelasticity, on the other hand, is sensitive to differences of principle stresses, i.e., photoelastic fringes are contours of equal $\sigma_1 - \sigma_2$, where σ_1 and σ_2 are the two in-plane principal stresses in plane stress. For CGS fringes, the expression for $(\sigma_{11}+\sigma_{22})_{,1}$ is given by

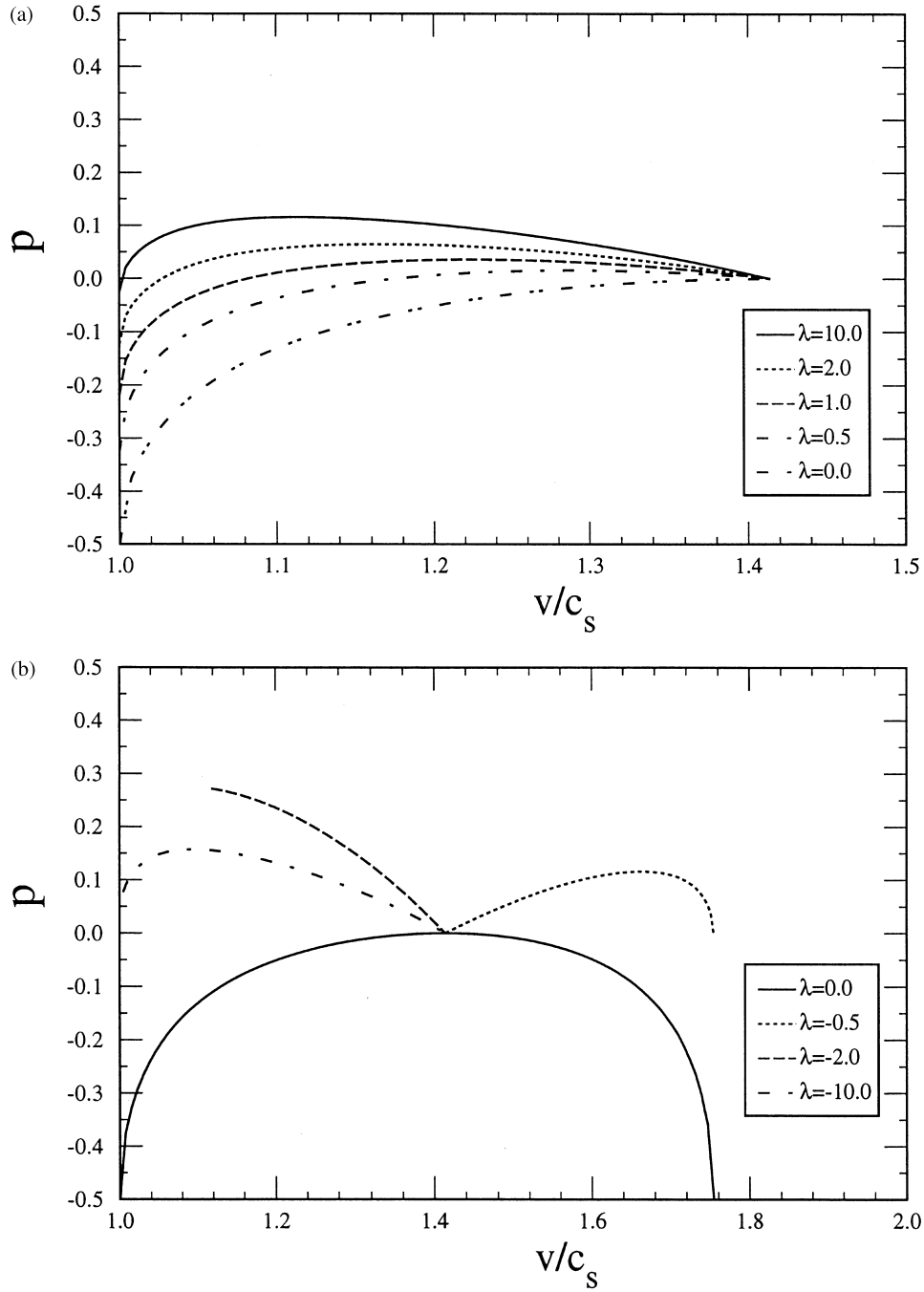

Fig. 5. The power of stress singularity p at the end of the contact zone vs the normalized crack tip velocity, v/c_s, for a plane-stress PMMA/rigid bimaterial system (Poisson's ratio $\nu_{PMMA} = 0.35$) : (a) positive linear contact coefficients λ ; (b) admissible negative linear contact coefficients λ.

$$(\sigma_{11}+\sigma_{22})_{,1} = -\frac{2\mu(\alpha_l^2+\hat{\alpha}_s^2)}{1+\alpha_l^2\hat{\alpha}_s^2}\sum_{n=0}^{\infty} B_n r_1^{n-q-1}\, r_2^{-p-1}$$

$$\cdot\{\alpha_l\hat{\alpha}_s(q-n)r_2\cos[(q-n+1)\theta_1+p\theta_2]+(q-n)r_2\sin[(q-n+1)\theta_1+p\theta_2],$$

$$+\alpha_l\hat{\alpha}_s p r_1\cos[(q-n)\theta_1+(p+1)\theta_2]+pr_1\sin[(q-n)\theta_1+(p+1)\theta_2]\} \quad (37)$$

where (r_1, θ_1) and (r_2, θ_2) are the scaled polar coordinates in $(\eta_1, \alpha_l\eta_2)$ plane, centered at the crack tip and the end of contact zone, respectively, and are given by

$$r_1 = \sqrt{\eta_1^2+\alpha_l^2\eta_2^2} \quad \theta_1 = \tan^{-1}(\alpha_l\eta_2/\eta_1), \quad (38a)$$

$$r_2 = \sqrt{(\eta_1+l)^2+\alpha_l^2\eta_2^2} \quad \theta_2 = \tan^{-1}[\alpha_l\eta_2/(\eta_1+l)]. \quad (38b)$$

For photoelasticity fringes, $\sigma_1-\sigma_2 = [(\sigma_{11}-\sigma_{22})^2+4\sigma_{12}^2]^{1/2}$ can be obtained from Eq. (34).

Figures 6(a) and (b) show the comparison between synthetically and experimentally obtained CGS fringe patterns for a crack tip velocity of $v = 1300$ m/s. The contact length cannot be accurately measured from the experimental fringe pattern because the end of the contact zone is not clearly identified in Fig. 6(b). However, the contact zone length l is estimated between 1.5 and 2.0 mm. The corresponding synthetic fringes are obtained by choosing the value of $v = 1300$ m/s from experiments and choosing the contact length l (between 1.5 and 2.0 mm), the linear contact coefficient λ and the amplitude parameters $B_0, B_1, \ldots B_n, \ldots$ so that a best fit is obtained. In this particular comparison only two non-zero amplitude parameters (B_0, B_1) were fitted, and λ and l are taken as $\lambda = 10$ and $l = 1.85$ mm, respectively. As observed from comparison, the synthetic fringe pattern clearly exhibits existence of the two distinct singularities, one at the crack tip and the other at the end of the contact zone. This is shown in the form of two distinct "circular" sets of fringes separated by a distance l along the interface.

The existence of two distinct shock waves, one emanating from the crack tip and the other from the end of the contact zone is clearly evident in Figs. 7(a) and (b), where a photoelastic fringe pattern is compared with the theory. Here the crack tip is propagating with velocity $v = 1.2c_s$ as measured in experiments. The linear contact coefficient λ is fixed at 10, and only one non-zero amplitude parameter (B_0) is used. The predicted shock wave corresponding to the crack tip appears stronger than one emanating from the end of the contact zone. This reflects the generally weaker singularity existing at that location.

6. ENERGY DISSIPATION RATE AND PROPOSED FRACTURE CRITERION

General energy considerations

One of the peculiar features of intersonic, shear-dominated crack growth in both homogeneous and bimaterial systems is the existence of crack tip singularity exponents that are less than 1/2 for most of the crack tip velocity regime, and may reach 1/2

only at $\sqrt{2}c_s$ in a homogeneous system. This phenomenon has been well documented in a series of investigations (e.g., Freund, 1990; Broberg, 1989) for homogeneous systems. For intersonic crack growth in bimaterial systems, however, it is only recently that equivalent observations were made in relation to traction-free interfacial crack (Liu *et al.*, 1995; Yu and Yang, 1995, Huang *et al.*, 1996). For this particular problem, the stress singularity exponent was found to remain well below 0.4 for the entire velocity regime. The immediate implication of the above observation is that the corresponding crack tip energy release rate vanishes as long as the singularity exponent is less than 1/2.

For the case of intersonic bi-lateral slip in homogeneous materials (shear-dominated intersonic crack growth), Broberg (1989) introduced a process zone model of Dugdale–Barenblatt type to remedy the pathology of zero crack tip energy release rate, when crack tip velocities were different from $\sqrt{2}c_s$. This provides an energy absorption mechanism near the crack tip. Our contact zone model, although not of the cohesive zone type, bears substantial similarity to this work and also provides an alternative mechanism of energy absorption. However, our model is, in addition, directly motivated by experimental observations of large scale crack face contact and the associated double shock wave creation. Such shock waves are characteristic of an intersonically moving contact region and is not expected in classical models of the Dugdale–Barenblatt type.

Direct application of the dynamic J integral and energy flux concepts in Freund (1990) combined with the existence of zero energy release rate at the crack tip provides the following expression for the net energy flow into the entire crack tip/contact zone region,

$$J = D + G, \tag{39}$$

where D is the energy dissipation over the contact zone per unit crack length and is given by

$$D = \int_{-l}^{0} (-\sigma_{12}) \frac{\partial u}{\partial \eta_1} \mathrm{d}\eta_1 \quad \text{at } \eta_2 = 0^+, \tag{40}$$

while G is the energy release rate at the crack tip and vanishes

$$G = 0 \tag{41}$$

By substitution of the general solution in Eqs. (34) and (35), we get

$$D = \frac{\mu\alpha_l^2(1+\hat{\alpha}_s^2)^2\lambda(1-\hat{\alpha}_s^2)(1+\lambda\hat{\alpha}_s)\displaystyle\int_0^l \frac{\left[\sum_{n=0}^{\infty}(-1)^n B_n \eta^n\right]^2}{\eta^{2q}(l-\eta)^{2p}}\mathrm{d}\eta}{[\alpha_l^2\hat{\alpha}_s(1+\hat{\alpha}_s^2)+\lambda(1-\hat{\alpha}_s^2+2\alpha_l^2\hat{\alpha}_s^2)]^2+[\alpha_l(1+\hat{\alpha}_s^2)(1+\lambda\hat{\alpha}_s)]^2}. \tag{42}$$

From the above expression, one can see that the requirement of non-negative energy dissipation is equivalent to the requirement that the shear tractions resist crack face sliding, see Eq. (23). The dominant, leading term of the above expression is given by

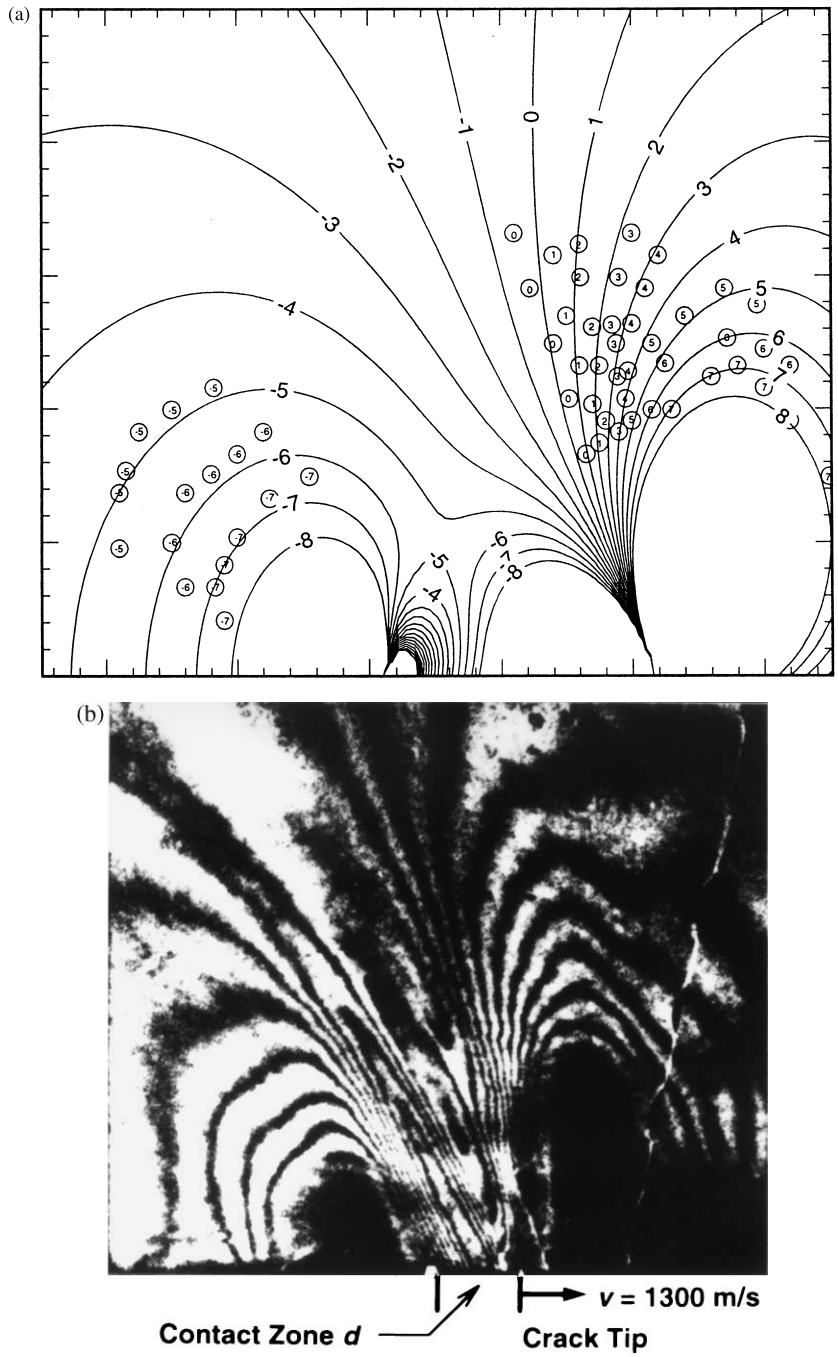

Fig. 6. Comparison between synthetically and experimentally obtained CGS fringe patterns for a crack tip velocity of $v = 1300$ m/s, $c_s = 1000$ m/s : (a) synthetically obtained CGS fringe patterns for the plane-stress PMMA/rigid bimaterial system ; (b) experimentally obtained CGS fringe patterns (Lambros and Rosakis, 1995) for the PMMA/steel bimaterial system ; the length of the contact zone is approximately 2 mm.

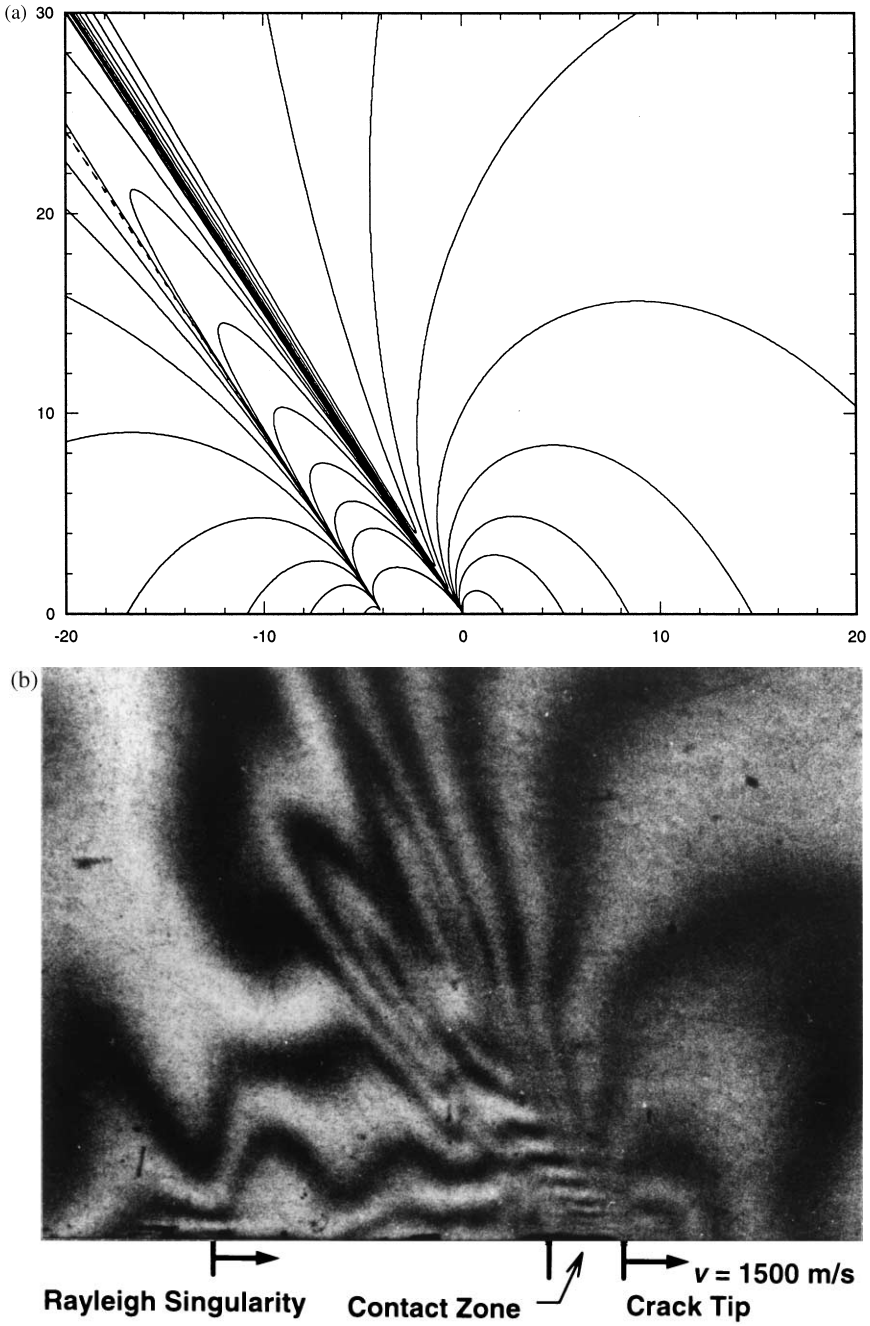

Fig. 7. Comparison between synthetically and experimentally obtained photoelasticity fringe patterns for a crack tip velocity of $v = 1.2c_s$: (a) synthetically obtained photoelasticity fringe patterns for the plane-stress Homalite/rigid bimaterial system; (b) experimentally obtained photoelasticity fringe patterns (Singh *et al.*, 1997) for the Homalite/steel bimaterial system; the length of the contact zone is approximately 2 mm.

$$D = \frac{B_0^2}{l^{2(q+p)-1}} \cdot \frac{\mu\alpha_l^2(1+\hat{\alpha}_s^2)^2\lambda(1-\hat{\alpha}_s^2)(1+\lambda\hat{\alpha}_s)\beta(1-2q, 1-2p)}{[\alpha_l^2\hat{\alpha}_s(1+\hat{\alpha}_s^2)+\lambda(1-\hat{\alpha}_s^2+2\alpha_l^2\hat{\alpha}_s^2)]^2+[\alpha_l(1+\hat{\alpha}_s^2)(1+\lambda\hat{\alpha}_s)]^2}, \quad (43)$$

where

$$\beta(a, b) = \int_0^1 x^{a-1}(1-x)^{b-1}\,dx \quad (44)$$

is the β-function, and B_0 is an unknown function of the crack tip velocity, linear contact coefficient, bimaterial properties, and external loading.

Critical sliding displacement failure criterion

In order to further investigate the nature of energy dissipation and energy flux, we need to introduce an additional postulate (criterion) of dynamic crack growth which provides additional information regarding the unknown amplitude factor appearing in Eq. (43). Recent analytical and experimental work on dynamic subsonic interfacial crack growth has shown that a viable dynamic crack growth criterion for the subsonic regime can be based on the attainment of constant crack opening and sliding displacements at the end of the crack tip cohesive zone (Fey and Rosakis, 1997a, b). This work makes use of a dynamic cohesive zone model of Dugdale–Barenblatt type. The model is used to interpret subsonic experimental results and to calculate the critical values of opening and sliding displacements in the entire subsonic regime. Based on the experimental data, these critical displacements are found to be time and velocity invariant.

Motivated by the above subsonic criterion, and in the absence of opening displacements in the contact zone in the present model, we postulate here that intersonic crack growth will take place in the presence of a critical sliding displacement evaluated at the end of the contact zone, i.e.,

$$u_1(\eta_1 = -l, \eta_2 = 0^+) = \delta_c, \quad (45)$$

where δ_c is a time and velocity invariant which depends only on bimaterial and bond properties. It should be pointed out that, although the above postulation is a natural generalization of the dynamic crack growth criterion for the subsonic regime (Fey and Rosakis, 1997a, b), it needs to be verified by experiments. However, some concluding remarks based on this postulation, as discussed in the following, will aid the comparison with future experiments.

The above equation determines the amplitude B_0 in terms of the critical sliding displacement δ_c, crack tip velocity v, linear contact coefficient λ, and contact length l as follows,

$$B_0 = -\frac{\delta_c l^{p+q-1}}{\beta(1-q, 1-p)\sin q\pi}. \quad (46)$$

Substituting Eq. (46) into Eq. (43), we obtain

$$\frac{D}{\mu\delta_c^2/l} = \frac{\beta(1-2q, 1-2p)}{(\sin q\pi)^2[\beta(1-q, 1-p)]^2} \cdot \frac{\lambda\alpha_l^2(1+\hat{\alpha}_s^2)^2(1-\hat{\alpha}_s^2)(1+\lambda\hat{\alpha}_s)}{[\alpha_l^2\hat{\alpha}_s(1+\hat{\alpha}_s^2)+\lambda(1-\hat{\alpha}_s^2+2\alpha_l^2\hat{\alpha}_s^2)]^2+[\alpha_l(1+\hat{\alpha}_s^2)(1+\lambda\hat{\alpha}_s)]^2}. \quad (47)$$

Its left hand side is the normalized energy dissipation rate, and its velocity dependence is plotted in Figs. 8(a–c) for three different ranges of admissible linear contact coefficient λ in Fig. 3. Figure 8(a) gives the normalized dissipation rate for positive λ. This corresponds to region I of Fig. 3 for admissible λ. The energy dissipation rate D is found to be finite in the velocity range from c_s to $\sqrt{2}c_s$, provided that λ remains finite. Its maximum occurs at c_s and monotonically decreases to zero at $\sqrt{2}c_s$. The existence of the maximum seems to suggest that there is an energy barrier of finite strength at the velocity c_s. This may be consistent with experimental observations (Liu *et al.*, 1993; Lambros and Rosakis, 1995; Singh *et al.*, 1997) that crack seems to favor growth at $v = c_s$ and remain at this speed for a substantial period during the experiments. However, when cracks velocities increase above c_s, they do so in a highly unstable manner (acceleration on the order of 10^8 m/s^2). Indeed, the unstable crack growth is consistent with the need of decreasing energy dissipation for higher crack tip speed (Fig. 8(a)).

Figure 8b gives the same plot for $-\infty < \lambda < -1$. This corresponds to the region II of Fig. 3 for admissible linear contact coefficient λ. The main difference of this figure with Fig. 8(a) is that, for each coefficient $\lambda < -1$, there exists a crack tip speed, $v^* = [c_s(\sqrt{1+(1/\lambda^2)})]$, for which the energy dissipation rate becomes infinite (see vertical asymptotes). To the left of the asymptote, stable crack growth is inadmissible on the basis of Eq. (13). For negative λ, the existence of an infinite energy barrier probably precludes the attainment of crack tip speed beyond the vertical asymptote. However, experiments have clearly shown crack tip speeds as high as $1.4c_s$ (Lambros and Rosakis, 1995). Consequently, the above result implies that either negative coefficients λ were not present in these experiments, or that the restriction only holds for steady-state crack growth.

Figure 8(c) corresponds to the linear contact coefficient $-1 < \lambda < 0$, region III of Fig. 3 for admissible λ. The admissible λ in this range all corresponds to crack tip speed larger than $\sqrt{2}c_s$. It is conceivable that above $\sqrt{2}c_s$, contact may still exist, depending on the external loading which will dictate the sign of the undetermined coefficient B_0. However, if that happens, the coefficient λ is restricted to be within region III in Fig. 3. If the above conditions are met, the required energy dissipation rate increases with velocity (stable crack growth), and in certain cases, becomes infinite at $v^* = [c_s(\sqrt{1+(1/\lambda^2)})]$ for $-1 < \lambda < -[(\kappa-1)/2]^{1/2}$. The predicted infinite energy barrier then implies the existence of a terminal speed v^* given above. However, for $-[(\kappa-1)/2]^{1/2} < \lambda < 0$, the energy dissipation rate D remains finite and the crack tip speed may exceed the longitudinal wave speed c_l of the elastic solid.

It should be emphasized at this point that the present solution is incapable of predicting the exact nature of intersonic crack growth. Because of its asymptotic and steady-state nature (no far field boundary conditions are prescribed) it involves undetermined amplitude constants. In addition the length, l, of the contact zone is

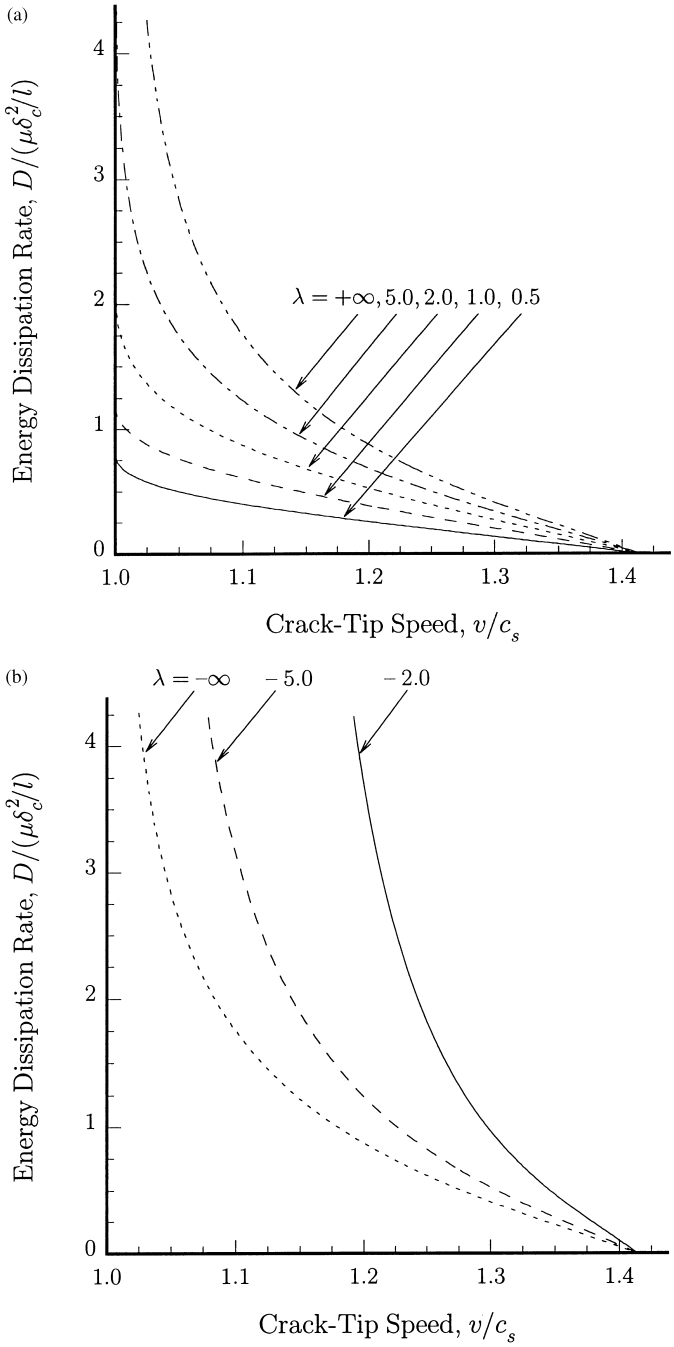

Fig. 8. The normalized energy dissipation rate, vs the crack tip velocity, v/c_s, for a plane-stress PMMA/rigid bimaterial system (Poisson's ratio $\nu_{\text{PMMA}} = 0.35$): (a) positive admissible linear contact coefficient λ, corresponding to region I in Fig. 3; (b) negative admissible λ in the range $-\infty < \lambda < -1$, corresponding to region II in Fig. 3; (c) negative admissible λ in the range $-1 < \lambda < 0$, corresponding to region III in Fig. 3.

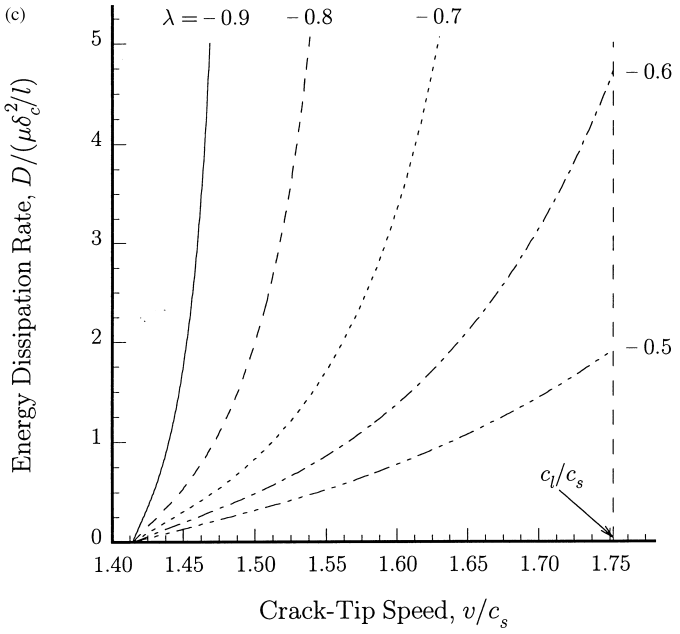

Fig. 8 *Continued.*

not by any way restricted to depend on these amplitudes or on the crack tip speed, and it is intensionally kept arbitrary. This is a major difference to static or dynamic cohesive zone models where the requirement of zero singularity at the crack tip produces a relationship between the length of the cohesive zone, the crack tip speed and the far-field stress intensity factor. Here we have intensionally refrained from imposing an equivalent restriction since we felt that the experiments clearly showed evidence of a non-vanishing crack tip singularity. The solution also does not provide conclusive information regarding terminal crack tip speeds. It only gives indications of possible acceptable scenarios (admissible regimes of intersonic crack growth which only weakly restrict the crack tip behavior within the specific ranges of admissible linear contact coefficients and the requirement of steady state crack growth). In other words it investigates the admissible solution space, within which many possible intersonic crack growth scenarios may exist in physical reality.

7. SUMMARY OF RESULTS

The paper describes an analytical model of intersonic crack propagation along the interface of an elastic/rigid bimaterial accounting for large scale crack face contact. The analysis predicts the essential features observed in CGS and photoelasticity experiments. These include two distinct velocity dependent singularities at the crack tip and at the trailing end of the contact region, as well as the appearance of two

distinct shock waves emanating from these two points. Appropriate choice of stress field and contact parameters result in synthetic fringe patterns that compare very favorably with experimental counterparts. The solution also allows for the calculation of the rate of energy dissipation resulting from crack face contact as a function of crack tip speed, contact length, and linear contact coefficient. A simple fracture criterion based on the attainment of critical crack face sliding displacement at the end of the contact zone is used to investigate the mechanism of energy dissipation at various intersonic crack tip speeds.

ACKNOWLEDGEMENTS

Y.H. and A.J.R. acknowledge insightful discussions with Dr J. R. Rice. Y.H. gratefully acknowledges the support from National Science Foundation (Grant No. INT-94-23964 and No. CMS-96-10491) and from ALCOA Foundation. C.L. acknowledges the Director Funded Postdoctoral Fellowship at Los Alamos National Laboratory. A.J.R. acknowledges the support from ONR (Grant No. N00014-95-1-0453) and NSF (Grant No. MSS-90-24838).

REFERENCES

Atkinson, C. (1977) Dynamic crack problems in dissimilar media. *Mechanics of Fracture* **4,** 213–248. Noordhoff, Leyden.

Broberg, K. B. (1989) The near-tip field at high crack velocities. *International Journal of Fracture* **39,** 1–13.

Brock, L. M. and Achenbach, J. D. (1973) Extension of an interface flaw under the influence of transient waves. *International Journal of Solids and Structures* **9,** 53–67.

Deng, X. (1992) Complete complex series expansions of near-tip fields for steadily growing interface cracks in dissimilar isotropic materials. *Engineering Fracture Mechanics* **42,** 237–242.

Fey, K. and Rosakis, A. J. (1997a) A cohesive zone model for dynamic crack growth along a bimaterial surface, Part I : analytical development, submitted for publication.

Fey, K. and Rosakis, A. J. (1997b) A cohesive zone model for dynamic crack growth along a bimaterial interface, Part II : experimental verification and a local crack growth criterion, submitted for publication.

Freund, L. B. (1972) Energy flux into the tip of an extending crack in an elastic solid. *Journal of Elasticity* **2,** 341–349.

Freund, L. B. (1979) The mechanics of dynamic shear crack propagation. *J. Geophys. Res.* **84,** 2199–2209.

Freund, L. B. (1990) *Dynamic Fracture Mechanics*. Cambridge University Press, Cambridge.

Georgiadis, H. G. and Barber, J. R. (1993a) On the super-Rayleigh/subseismic elastodynamic indentation problem. *Journal of Elasticity* **31,** 141–161.

Georgiadis, H. G. and Barber, J. R. (1993b) Steady-state transonic motion of a line load over an elastic half-space : the corrected Cole/Huth solution. *Journal of Applied Mechanics* **60,** 772–774.

Gol'dstein, R. V. (1967) On surface waves in jointed elastic materials and their relation to crack propagation along the junction. *Appl. Math. Mech.* **31,** 496–502.

Huang, Y., Liu, C. and Rosakis, A. J. (1996) Transonic crack growth along a bimaterial interface : an investigation of the asymptotic structure of near-tip fields. *International Journal of Solids and Structures* **33**(18), 2625–2645.

Lambros, J. and Rosakis, A. J. (1995) Shear dominated transonic crack growth in a bima-

terial—I. Experimental observations. *Journal of the Mechanics and Physics of Solids* **43**(2), 169–188.
Liu, C., Huang, Y. and Rosakis, A. J. (1995) Shear dominated transonic crack growth in a bimaterial—II. Asymptotic fields and favorable velocity regimes. *Journal of the Mechanics and Physics of Solids* **43**(2), 189–206.
Liu, C., Lambros, J. and Rosakis, A. J. (1993) Highly transient elasto-dynamic crack growth in a bimaterial interface: higher order asymptotic analysis and optical experiment. *Journal of the Mechanics and Physics of Solids* **41**(12), 1887–1954.
Perrin, G., Rice, J. R. and Zheng, G. (1995) Self-healing slip pulse on a frictional surface. *Journal of the Mechanics and Physics of Solids* **43**(9), 1461–1495.
Prakash, V. and Clifton, R. J. (1992) Pressure-shear plate impact measurement of dynamic friction for high speed machining applications. In *Proceedings of VII International Congress on Experimental Mechanics*, *Las Vegas*, *June* 1992, 556–564. Soc. Exp. Mech., Bethel, CT.
Prakash, V. and Clifton, R. J. (1993) Time-resolved dynamic friction measurements in pressure-shear. In *Experimental Techniques in the Dynamics of Deformable Solids*, Vol. 165, pp. 33–48. Applied Mechanics Div., ASME, New York.
Rice, J. R. (1988) Elastic fracture mechanics concepts for interface cracks. *Journal of Applied Mechanics* **55,** 98–103.
Singh, R. P., Lambros, J., Shukla, A. and Rosakis, A. J. (1997) Investigation of the mechanics of intersonic crack propagation along a bimaterial interface using coherent gradient sensing and photoelasticity. *Proceedings of the Royal Society*, accepted for publication.
Tippur, H. V. and Rosakis, A. J. (1991) Quasi-static and dynamic crack growth along bimaterial interfaces: a note on crack-tip field measurement using coherent gradient sensing. *Exp. Mech.* **31**(3), 243–251.
Wang, W., Huang, Y., Rosakis, A. J. and Liu, C. (1997) Effect of elastic mismatch in intersonic crack propagation along a bimaterial interface. Submitted for publication.
Willis, J. R. (1971) Fracture mechanics of interfacial cracks. *Journal of the Mechanics and Physics of Solids* **19,** 353–368.
Willis, J. R. (1973) Self-similar problems in elastodynamics. *Phil. Trans. R. Soc. Lond.* **274,** 435–491.
Wu, K. C. (1991) Explicit crack-tip fields of an extending interface crack in an anisotropic bimaterial. *International Journal of Solids and Structures* **27,** 455–466.
Xu, X.-P. and Needleman, A. (1996) Numerical solutions of dynamic crack growth along an interface. *International Journal of Fracture* **74,** 289–324.
Yang, W., Suo, Z. and Shih, C. F. (1991) Mechanics of dynamic debonding. *Proceedings of the Royal Society of London* **A433,** 679–697.
Yu, H. and Yang, W. (1994) Mechanics of transonic debonding of a bimaterial interface: the anti-plane shear case. *Journal of the Mechanics and Physics of Solids* **42,** 1789–1802.
Yu, H. and Yang, W. (1995) Mechanics of transonic debonding of a bimaterial interface: the inplane case. *Journal of the Mechanics and Physics of Solids* **43,** 207–232.

APPENDIX

The asymptotic fields near a crack tip

The asymptotic displacement and stress fields near a crack tip are given by

$$\begin{pmatrix} u_1 \\ u_2 \end{pmatrix} = \frac{A_0}{1+\alpha_l^2\hat{\alpha}_s^2} \cdot \frac{1}{1-q} \cdot \left\{ r_l^{1-q} \left[\cos(1-q)\theta_l \begin{pmatrix} \alpha_l\hat{\alpha}_s \\ -\alpha_l \end{pmatrix} - \sin(1-q)\theta_l \begin{pmatrix} 1 \\ \alpha_l^2\hat{\alpha}_s \end{pmatrix} \right] \right.$$
$$\left. -\alpha_l|\eta_1+\hat{\alpha}_s\eta_2|^{1-q} \begin{pmatrix} \hat{\alpha}_s \\ -1 \end{pmatrix} [H(\eta_1+\hat{\alpha}_s\eta_2) - (\cos q\pi - \alpha_l\hat{\alpha}_s \sin q\pi) H(-\eta_1-\hat{\alpha}_s\eta_2)] \right\}, \quad \text{(A1)}$$

and

$$\begin{bmatrix}\sigma_{11}\\ \sigma_{22}\\ \sigma_{12}\end{bmatrix} = \frac{\mu A_0}{1+\alpha_l^2\hat{\alpha}_s^2}\left\{\frac{1}{r_1^q}\begin{bmatrix}(1+2\alpha_l^2+\hat{\alpha}_s^2)(\alpha_l\hat{\alpha}_s\cos q\theta_1+\sin q\theta_1)\\ (-1+\hat{\alpha}_s^2)(\alpha_l\hat{\alpha}_s\cos q\theta_1+\sin q\theta_1)\\ -2\alpha_l(\cos q\theta_1-\alpha_l\hat{\alpha}_s\sin q\theta_1)\end{bmatrix}\right.$$

$$\left.+\frac{\alpha_l}{|\eta_1+\hat{\alpha}_s\eta_2|^q}[H(\eta_1+\hat{\alpha}_s\eta_2)+(\cos q\pi-\alpha_l\hat{\alpha}_s\sin q\pi)H(-\eta_1-\hat{\alpha}_s\eta_2)]\begin{bmatrix}-2\hat{\alpha}_s\\ 2\hat{\alpha}_s\\ 1-\hat{\alpha}_s^2\end{bmatrix}\right\}, \quad \text{(A2)}$$

where $H(\cdot)$ is the Heaviside step function, (r_1, θ_1) are the scaled polar coordinates in $(\eta_1, \alpha_l\eta_2)$ plane, and are given by

$$r_1 = \sqrt{\eta_1^2+\alpha_l^2\eta_2^2} \quad \theta_1 = \tan^{-1}(\alpha_l\eta_2/\eta_1). \quad \text{(A3)}$$

The functions s_{ij} *in Eq.* (33) *for the finite contact zone solution*

The functions s_{ij} in Eq. (33) for the finite contact zone solution are given by

$$\begin{bmatrix}s_{11}(\eta_1,\eta_2,q,p)\\ s_{22}(\eta_1,\eta_2,q,p)\\ s_{12}(\eta_1,\eta_2,q,p)\end{bmatrix} = \frac{1}{1+\alpha_l^2\hat{\alpha}_s^2}$$

$$\cdot\left\{\frac{1}{r_1^q r_2^p}\begin{bmatrix}(1+2\alpha_l^2+\hat{\alpha}_s^2)[\alpha_l\hat{\alpha}_s\cos(q\theta_1+p\theta_2)+\sin(q\theta_1+p\theta_2)]\\ -(1-\hat{\alpha}_s^2)[\alpha_l\hat{\alpha}_s\cos(q\theta_1+p\theta_2)+\sin(q\theta_1+p\theta_2)]\\ -2\alpha_l[\cos(q\theta_1+p\theta_2)-\alpha_l\hat{\alpha}_s\sin(q\theta_1+p\theta_2)]\end{bmatrix}\right.$$

$$-\frac{1}{|\eta_1+\hat{\alpha}_s\eta_2|^q\cdot|\eta_1+\hat{\alpha}_s\eta_2+l|^p}[\alpha_l H(\eta_1+\hat{\alpha}_s\eta_2)+\alpha_l(\cos\pi q-\alpha_l\hat{\alpha}_s\sin\pi q),$$

$$\cdot(H(\eta_1+\hat{\alpha}_s\eta_2+l)-H(\eta_1+\hat{\alpha}_s\eta_2))+\frac{(1-\hat{\alpha}_s^2)}{2\hat{\alpha}_s}$$

$$\left.\cdot(\alpha_l\hat{\alpha}_s\cos\pi(q+p)+\sin\pi(q+p))H(-\eta_1-\hat{\alpha}_s\eta_2-l)]\begin{pmatrix}2\hat{\alpha}_s\\ -2\hat{\alpha}_s\\ -1+\hat{\alpha}_s^2\end{pmatrix}\right\} \quad \text{(A4)}$$

where (r_1, θ_1) and (r_2, θ_2) are the scaled polar coordinates in $(\eta_1, \alpha_l\eta_2)$ plane, centered at the crack tip and the end of contact zone, respectively, and are given in Eq. (38).